Evaluation of computed tomographic anatomy of the equine metacarpophalangeal joint

Katrien Vanderperren, DVM; Benoit Ghaye, MD; Frédéric R. Snaps, DVM, PhD; Jimmy H. Saunders, DVM, PhD

Objective—To determine the detailed computed tomography (CT) anatomy of the metacarpophalangeal (MCP) joint in healthy horses.

Sample Population—10 cadaveric forelimbs from 10 adult horses without orthopedic disease.

Procedures—CT of the MCP joint was performed on 4 forelimbs. In 1 of the limbs, CT was also performed after intra-articular injection of 30 mL of contrast medium (40 mg of iodine/mL). Transverse slices 1-mm thick were obtained, and sagittal and dorsal planes were reformatted with a slice thickness of 2 mm. The CT images were matched with corresponding anatomic slices from 6 additional forelimbs.

Results—The third metacarpal bone, proximal sesamoid bones, and proximal phalanx could be clearly visualized. Common digital extensor tendon; accessory digital extensor tendon; lateral digital extensor tendon; superficial digital flexor tendon (including manica flexoria); deep digital flexor tendon; branches of the suspensory ligament (including its attachment); extensor branches of the suspensory ligament; collateral ligaments; straight, oblique, and cruciate distal sesamoidean ligaments; intersesamoidean ligament; annular ligament; and joint capsule could be seen. Collateral sesamoidean ligaments and short distal sesamoidean ligaments could be localized but not at all times clearly identified, whereas the metacarpointersesamoidean ligament could not be identified. The cartilage of the MCP joint could be assessed on the postcontrast sequence.

Conclusions and Clinical Relevance—CT of the equine MCP joint can be of great value when results of radiography and ultrasonography are inconclusive. Images obtained in this study may serve as reference for CT of the equine MCP joint. (*Am J Vet Res* 2008;69:631–638)

The role of CT in veterinary practice is growing gradually because of the decrease in cost of equipment and increase in scanner availability. This imaging modality is especially useful for orthopedic problems for which fast diagnosis and complete understanding of the extent of disease is necessary.[1] The MCP joint is an important source of lameness in all types of horses and has been extensively studied with radiography and ultrasonography.[2,3] Inconclusive findings obtained via radiography or ultrasonography create the necessity for cross-sectional imaging modalities such as CT and MRI.[1,4–8] The main advantages of CT and MRI, compared with radiography and ultrasonography, are the simultaneous imaging of bone and soft tissue structures, the absence of superimposition, and the possibility of 3- dimensional imaging obtained either by reconstruction (CT) or at acquisition (MRI).[9–11] These techniques also have disadvantages, such as the need for general anesthesia, the need for a dedicated table, and the high purchase (MRI) and maintenance costs.[7,10,12] Advantages of CT, compared with MRI, are the better bone imaging and typically shorter examination time, whereas MRI is superior for evaluation of soft tissues and meta-

Abbreviations

CT	Computed tomography
MCP	Metacarpophalangeal
MRI	Magnetic resonance imaging
WW	Window width
HU	Hounsfield unit
WL	Window level
MCIII	Third metacarpal bone
SDFT	Superficial digital flexor tendon
DDFT	Deep digital flexor tendon

Received July 7, 2007.
Accepted October 18, 2007.
From the Department of Veterinary Medical Imaging and Small Animal Orthopaedics, Faculty of Veterinary Medicine, Ghent University, Salisburylaan 133, 9820 Merelbeke, Belgium (Vanderperren, Saunders); the Department of Medical Imaging, University Hospital Sart-Tilman, Domaine Universitaire du Sart-Tilman B 35, 4000 Liège, Belgium (Ghaye); and the Department of Clinical Sciences, Faculty of Veterinary Medicine, University of Liège, 4000 Liège, Belgium (Snaps).
Supported by the Research Foundation-Flanders (Belgium) (F.W.O.-Vlaanderen).
Presented as a poster at the Annual Conference of the European Association of Veterinary Diagnostic Imaging, Chalkidiki, Thessaloniki, Greece, August 29 to September 1, 2007.
The authors thank Patrick Vervaet and Kim Claus for technical assistance.
Address correspondence to Dr. Saunders.

bolic subchondral bone changes.[10] Standing low-field MRI performed with an open magnet can also be used and does not require general anesthesia, eases patient handling, and reduces the costs but results in lower resolution, longer imaging times, and requires the use of motion correction software.[13,14]

Computed tomographic arthrography of normal and diseased cartilage in the equine MCP joint,[a] the subchondral bone density and cartilage degeneration patterns in osteoarthritic metacarpal condyles,[15] and CT-angiography of the distal portion of the forelimb[16] have been described. Recently, intra-arterial contrast-enhanced CT of the distal portion of the limbs in horses has also been reported,[17] but to our knowledge, the CT anatomy of the normal equine MCP joint has not been published. The objective of the study reported here was to provide a detailed CT reference for the equine MCP joint.

Materials and Methods

Animals—Four adult horses (mean age, 13 years) euthanatized for reasons unrelated to the musculoskeletal system were studied. The horses were euthanatized with a combination[b] of embutramide, mebenzonium-iodide, and tetracaïne hydrochloride(4 to 6 mL/50 kg) injected IV via the vena jugularis.

Following euthanasia, 1 forelimb of each horse was severed at the level of the elbow joint. The 4 forelimbs had a normal appearance, and no abnormal findings were found on palpation. A standard radiographic examination (lateromedial, dorsopalmar, dorsolateral-palmaromedial oblique, and dorsomedial-palmarolateral oblique views) of the MCP joint of the 4 cadaveric forelimbs was made to confirm the absence of abnormal findings.

CT examinations—The CT examination of the MCP joint was obtained within 24 hours after euthanasia. The CT scans were performed with a 16-detector row CT scanner[c] in which the limbs were placed in the gantry to obtain transverse slices with the long axis of the limb parallel to the CT table. First, a scout image (120 kV, 160 mA) was performed to check for symmetry and to ensure that the entire region to be examined was included in the image. The forelimbs were scanned in a distal-to-proximal direction. Acquisition variables were 120 kV and 160 mA, 0.75-mm collimation, 0.6-mm increment, 1-second rotation time, a pitch of 0.85-1, field of view of 20 cm, matrix size of 512 × 512, and a pixel size of 0.39 mm. Transverse CT scans of 1-mm thickness were reconstructed from the proximal part of the palmar recess of the MCP joint to the proximal interphalangeal joint. The total time required for scanning of each forelimb was dependent on the length to be scanned and varied from 41.28 to 42.58 seconds. High–spatial-resolution kernel (U70u) for images visualized by use of bone windows settings and low–spatial resolution (U30u) for images visualized by use of soft tissues window settings were used. All images were reformatted from the same and unique data acquisition.

In 1 forelimb, an intra-articular injection of 30 mL of an iodinated (40 mg of I/mL) contrast medium[d] was performed to obtain a positive-contrast arthrograph of the MCP joint, and a new acquisition was obtained by use of the same variables.

All data were stored. From the images obtained before contrast medium administration, 2-mm thick (0.6-mm increment) sagittal and dorsal slices were reformatted by use of software.[e] Sagittal and dorsal images from all 4 forelimbs were reviewed by the use of a bone setting (WW = 3,200 HU; WL = 700 HU) and a soft tissue setting (WW = 280 HU; WL = 120 HU). Transverse planes were also reformatted from the transverse acquisition with a slice thickness of 2 mm (0.6-mm increment) and analyzed with a soft tissue setting (WW = 280 HU; WL = 120 HU). This was done to decrease the image noise present on the transverse images with a slice thickness of 1 mm. From the images obtained after contrast medium administration, sagittal and dorsal reconstructions were made and analyzed with a bone setting (WW = 3,200 HU; WL = 700 HU).

Comparison of CT and anatomic images—Six forelimbs of horses euthanatized for reasons unrelated to the musculoskeletal system were used to make the anatomic sections. For euthanasia, the same protocol[b] was used. Radiographic examination of the MCP joint of the anatomic specimens prior to sectioning was performed to confirm the absence of abnormal findings. Before making anatomic sections, the MCP joint was punctured with a 16-gauge needle and the synovial fluid was aspirated when present. The MCP joint was filled with a yellow pigment.[f] The limbs were frozen for at least 48 hours at –18°C, and each limb was cut in various planes (sagittal, dorsal, and transverse) in approximately 5- to 10-mm thick slices with an electric band saw.[g] Consequently, 6 forelimbs were necessary to produce the reference images.

All anatomic sections were photographed. For each anatomic slice, a corresponding CT image was chosen on the basis of similar appearance. Bony and soft tissue structures were identified on the anatomic sections and were subsequently located on the corresponding CT images. In addition, a published atlas was consulted.[18]

Results

Nine precontrast CT images (bone window with the corresponding soft tissue window) were selected (**Figure 1**) and matched with their corresponding anatomic section: 6 in a transverse plane (**Figure 2**), 2 in a dorsal plane (**Figure 3**), and 1 in a sagittal plane (**Figure 4**). Three postcontrast CT images were selected: 1 in a transverse and 2 in a sagittal plane (**Figure 5**).

With image WW and WL settings (WW = 3,200 HU; WL = 700 HU) adjusted for bone, all bone structures, including the diaphysis of MCIII, the condyles and the sagittal ridge of MCIII, the collateral fossae, the proximal sesamoid bones, and the proximal phalanx, were seen on transverse-, sagittal-, and dorsal-plane images. All images had excellent delineation between the cortex and medulla of the bones, and the trabecular structure was well depicted. Sagittal images allowed a detailed evaluation of the contour of the sagittal ridge and both condyles. The MCP joint could be evaluated in detail from the dorsal to palmar surface on the dorsal reconstructions.

The soft tissue structures that could be identified and evaluated on the different soft tissue window planes (WW = 280 HU; WL = 120 HU) included the common digital extensor tendon; accessory digital extensor tendon; lateral digital extensor tendon; SDFT (including manica flexoria); DDFT; branches of the suspensory ligament (including its attachment); extensor branches of the suspensory ligament; collateral ligaments; straight, oblique, and cruciate distal sesamoidean ligaments; intersesamoidean ligament; annular ligament; and the joint capsule (including the proximal synovial pad). The collateral sesamoidean ligaments and the short distal sesamoidean ligaments could be seen but not always clearly identified. The metacarpointersesamoidean ligament could not be identified.

The common and lateral digital extensor tendons were oval shaped on the transverse images and clearly seen. Between the common and lateral digital extensor tendons, a small oval structure was present and identified as the accessory digital extensor tendon. The extensor tendons were hyperattenuating, compared with the dorsal aspect of the joint capsule. The transverse images were best suited to identify the extensor tendons. The dorsal aspect of the joint capsule of the MCP joint, including the proximal synovial pad (a fold of fibrous connective tissue located in the dorsal recess of the joint capsule at its attachment to MCIII), could be seen as a hypoattenuating zone between the extensor tensor tendons and the dorsodistal aspect of MCIII. The joint capsule could be best identified on the transverse and sagittal reconstructions.

The lateral and medial collateral ligaments are composed of a superficial and a deep part. The superficial part originates proximally at the distal metacarpal shaft and attaches on the proximolateral-medial aspect

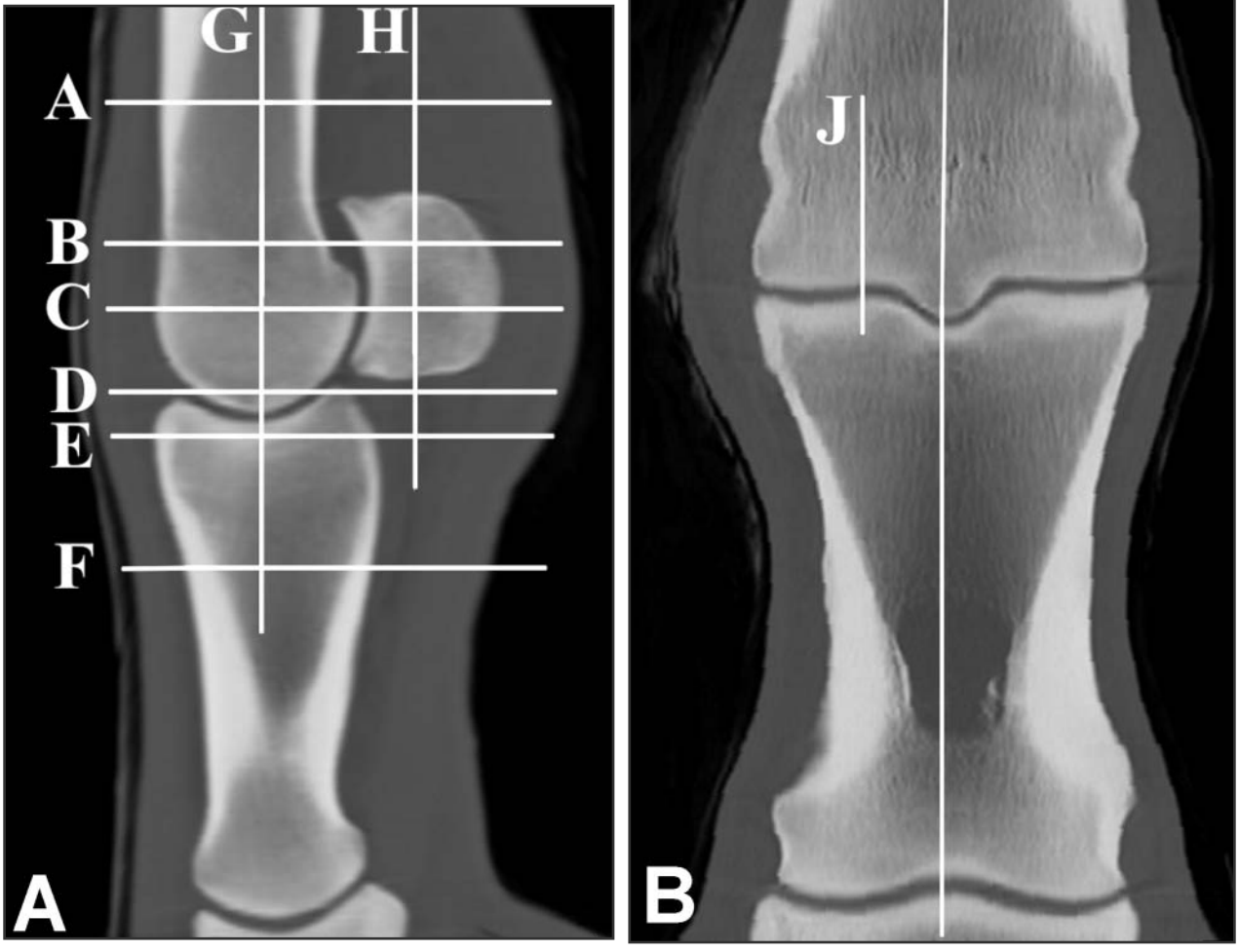

Figure 1—Two CT reconstructed views of a normal MCP joint in a horse. A—Sagittal CT reconstructed view. Selected sites (planes) for the transverse CT were the distal third of MCIII (A), the proximal third of the proximal sesamoid bones (B), the distal third of the proximal sesamoid bones (C), the MCP joint space (D, E), and the proximal aspect of the proximal phalanx (F). Selected sites (planes) for the reconstructed dorsal CT images were attachment sites of the collateral ligaments (G) and attachment sites of the distal sesamoidean ligaments at the proximal sesamoid bones (H). B—Dorsal CT reconstructed view. The view was reconstructed by use of the midsagittal (I) plane view obtained before and after intra-articular administration of contrast medium and the reconstructed parasagittal (J) plane view (medial to the sagittal ridge) after intra-articular administration of contrast medium.

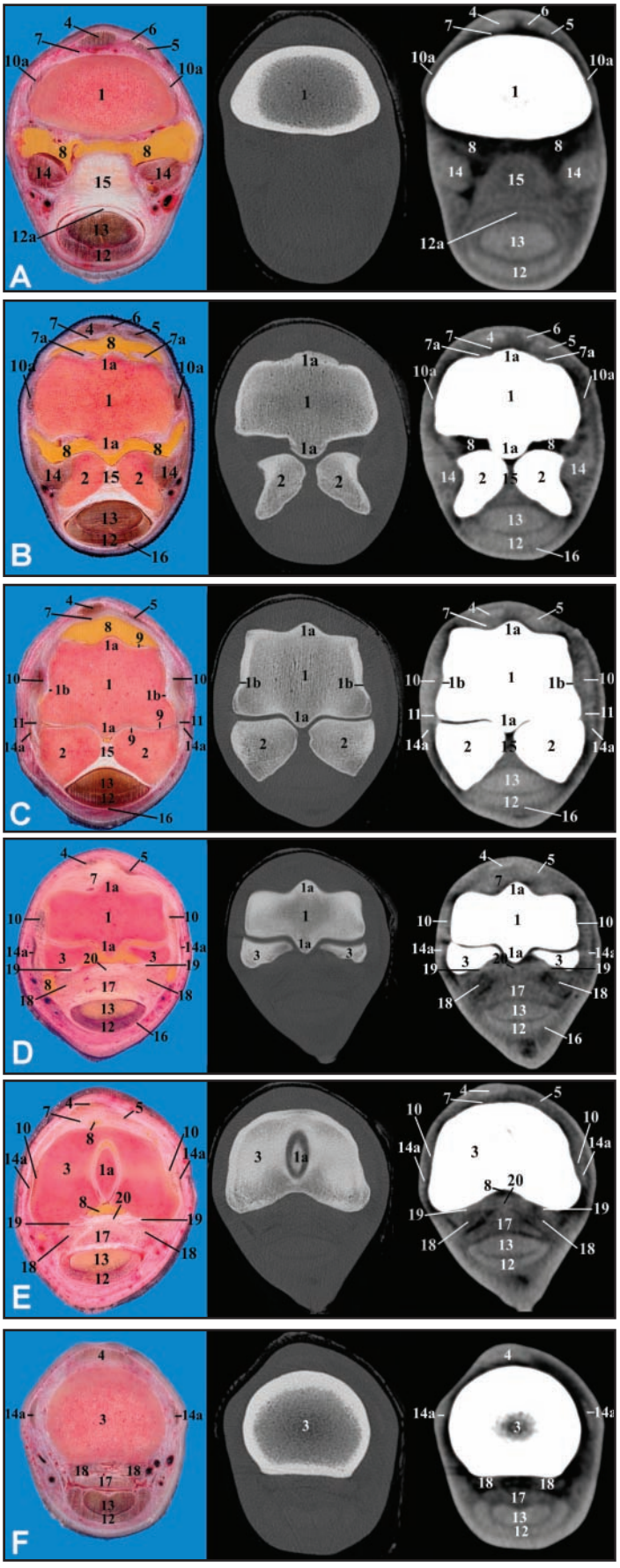

Figure 2—Photograph of a transverse anatomic section (left) and transverse CT views (middle: bone window; right: soft tissue window) of a normal MCP joint in a horse sequentially displayed from proximal to distal (A through F) as illustrated in Figure 1. Each image is orientated with the medial aspect to the left and the dorsal aspect to the top. 1 = MCIII. 1a = Sagittal ridge of MCIII. 1b = Collateral fossa. 2 = Proximal sesamoid bones. 3 = Proximal phalanx. 4 = Common digital extensor tendon. 5 = Lateral digital extensor tendon. 6 = Accessory digital extensor tendon. 7 = Joint capsule. 7a = Proximal synovial pad. 8 = Synovial recesses. 9 = Cartilage of the MCP joint. 10 = Collateral ligament. 10a = Superficial part of the collateral ligament. 10b = Deep part of the collateral ligament. 11 = Collateral sesamoidean ligament. 12 = SDFT. 12a = Manica flexoria. 13 = DDFT. 14 = Branches (medial branch: left; lateral branch: right) of the suspensory ligament. 14a = Extensor branches of the suspensory ligament. 15 = Intersesamoidean ligament. 16 = Annular ligament. 17 = Straight distal sesamoidean ligament. 18 = Oblique distal sesamoidean ligaments. 19 = Short distal sesamoidean ligaments. 20 = Cruciate distal sesamoidean ligaments.

of the proximal phalanx, running vertically. The triangular deep part begins at the abaxial condylar fossa and runs obliquely in a palmarodistal direction and inserts on the proximal phalanx and the proximal sesamoid bone. The superficial and deep parts of the collateral ligaments were best evaluated on the transverse and dorsal reconstructions. It was not possible to differentiate the soft tissue components of the superficial and deep parts. However, their separate sites of attachment were readily identified.

The lateral and medial collateral sesamoidean ligaments course from the abaxial surface of the proximal sesamoid bones to MCIII and the tuberosity of the proximal phalanx. These ligaments are superficial to the superficial part of the collateral ligaments and to the extensor branches of the suspensory ligament, which were hyperattenuating, compared with the collateral ligaments and the collateral sesamoidean ligaments. The collateral sesamoidean ligaments could be seen on the transverse images. On the dorsal images, the collateral sesamoidean ligaments could not be seen.

The flattened SDFT (on transverse images) was smoothly marginated, and its margins were clearly demarcated on the transverse, dorsal, and sagittal reconstructions. Proximal to the MCP joint, the manica flexoria of the SDFT, surrounding the DDFT, was clearly visualized. The DDFT, oval-shaped at the level of the MCP joint and bilobed in the proximal interphalangeal region, was seen in the 3 planes like the SDFT: smoothly marginated and with borders clearly differentiated. The SDFT and DDFT were denser, compared with the straight distal, oblique, cruciate, and short distal sesamoidean ligaments in the transverse, sagittal, and dorsal planes.

The lateral and medial branches of the suspensory ligament were round and became more trapezoid-shaped as they inserted at the apical and abaxial border of the proximal sesamoid bones. Both branches and the insertion of the suspensory branches at the proximal sesamoid bones were

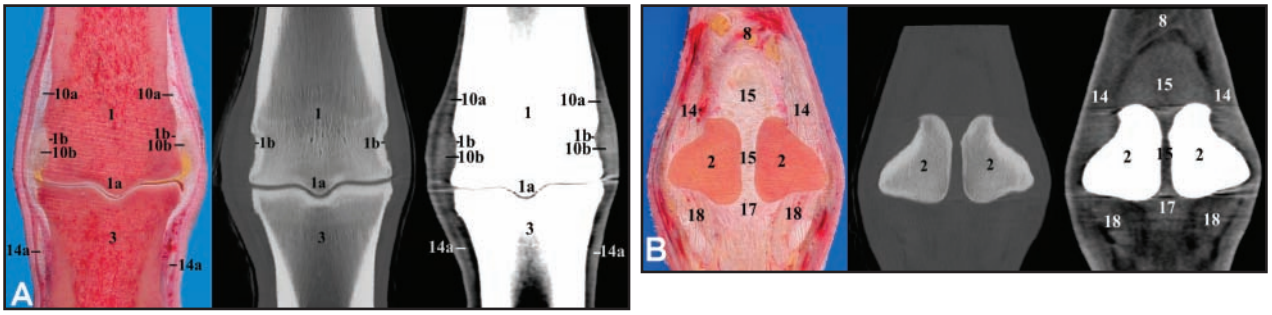

Figure 3—Photographs of selected dorsal anatomic sections (left) and dorsal reconstructed CT images (middle: bone window; right: soft tissue window) of the normal MCP joint in Figure 1A (A, B). Each image is orientated with the medial aspect to the left. *See* Figure 2 for key.

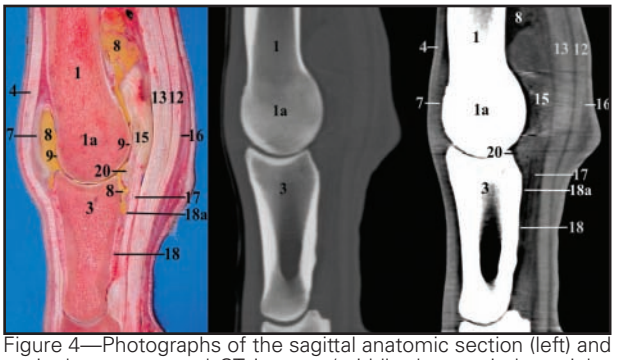

Figure 4—Photographs of the sagittal anatomic section (left) and sagittal reconstructed CT images (middle: bone window; right: soft tissue window) of the normal MCP joint in Figure 1 (I). Each image is orientated with the dorsal aspect to the left. 18a = Sagittal part of the oblique distal sesamoidean ligament. *See* Figure 2 for remainder of legend.

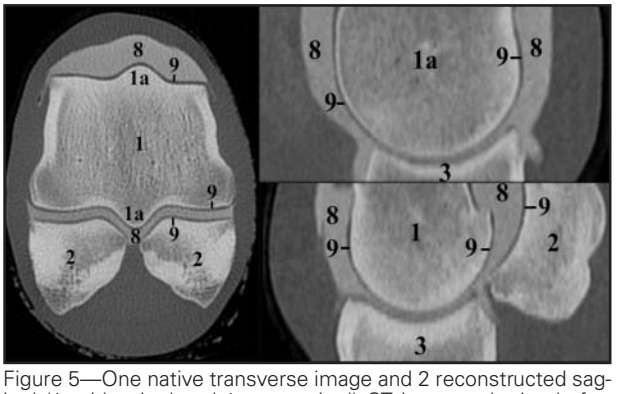

Figure 5—One native transverse image and 2 reconstructed sagittal (1 midsagittal and 1 parasagittal) CT images obtained after intra-articular administration of contrast medium in the MCP joint of a horse. The transverse image is oriented with the medial aspect to the left, and the sagittal images are oriented with the dorsal aspect to the left. The selected transverse image and the midsagittal CT images can be matched with the transverse anatomic section (Figure 2C) and with the midsagittal anatomic section (Figure 4). *See* Figure 2 for legend.

readily identifiable and well defined on the 3 reconstructions. The extensor branches of the suspensory ligament were hyperattenuating structures, compared with the surrounding structures, and could be best seen on the transverse and dorsal reconstructions. Between the 2 proximal sesamoid bones, the intersesamoidean ligament and fibrocartilage of the intersesamoidean ligament were well seen and had a homogeneous appearance. Between the 2 branches of the suspensory ligament and proximal sesamoid bones was the proximal palmar synovial recess of the MCP joint. This synovial recess had a heterogeneous appearance, compatible with fat, likely because of the synovial folds and synovial fluid. The thin annular ligament lying immediately under the skin and attaching to the abaxial surfaces of both proximal sesamoid bones could as well be identified and was seen on the sagittal and transverse planes.

The straight distal sesamoidean ligament originates from the base of the proximal sesamoid bones and the intersesamoidean ligament and inserts distally on the second phalanx where it forms, with the SDFT, the scutum medium. Proximally, the straight distal sesamoidean ligament had a trapezoidal shape; in the middle, a rectangular to square shape; and distally, became oval. Proximally, the clearly visible trapezoidal straight sesamoidean ligament had a homogeneous appearance and its borders were well demarcated. The middle part of the straight sesamoidean ligament had a heterogeneous appearance (Figures 2–4) and was poorly outlined. Running distally, the straight sesamoidean ligament was well defined and clearly outlined. On the sagittal and dorsal reconstructions, the origin and insertion of the straight sesamoidean ligament was clearly visualized.

The oblique distal sesamoidean ligament, which has 3 parts (lateral, sagittal, and medial), had separate origins from the base of the medial and lateral proximal sesamoid bones and the intersesamoidean ligament and attached on the palmar surface of the proximal phalanx. The oblique distal sesamoidean ligaments had a heterogeneous appearance. At the proximal part of the proximal phalanx, the lateral and medial oblique distal sesamoidean ligaments were well defined, although the separation with the short distal sesamoidean ligaments was rather difficult to discern. Differentiation between the sagittal part of the oblique distal sesamoidean ligament and the straight distal sesamoidean ligament was possible on the sagittal reconstruction. However, on the transverse planes, the sagittal part of the oblique distal sesamoidean ligament was not distinguishable from the straight distal sesamoidean ligament. In the middle of the proximal phalanx the oblique distal sesamoidean ligaments appeared as small triangular structures deep to the straight distal sesamoidean ligament adjacent to the bony surface of the proximal phalanx. The oblique distal sesamoidean ligaments were best evaluated on the transverse, sagittal, and dorsal reconstructions.

The cruciate distal sesamoidean ligaments lying under the straight and the oblique distal sesamoidean ligaments crossed from the axial part of the base of the proximal sesamoid bones to the contralateral

axial aspect of the palmar proximal phalanx, forming the palmar wall of the palmarodistal recess of the MCP joint. The cruciate distal sesamoidean ligaments were best evaluated on the transverse plane. On the sagittal reconstructions, the differentiation between the cruciate, oblique, and straight distal sesamoidean ligaments could not be made at the origin site on the base of the proximal sesamoid bones.

The short distal sesamoidean ligaments extend from the dorsal aspect of the base of the proximal sesamoid bones to the palmar margin of the articular surface of the proximal phalanx. The short distal sesamoidean ligaments were quite difficult to identify, resulting from the difficulty to differentiate them from the oblique sesamoidean ligaments. The separation between the short and oblique distal sesamoidean ligaments was best seen on the transverse images, although it was difficult to discern. The short distal sesamoidean ligaments were not recognizable as separate from the oblique sesamoidean ligaments in the sagittal planes.

The metacarpointersesamoidean ligament originates on the palmar distal aspect of MCIII and fuses with the intersesamoidean ligament. This ligament could not be identified.

The smooth cartilage of the MCP joint could be clearly assessed on the postcontrast transverse sequences. The cartilage of the dorsal and palmar aspect of MCIII and of the articular surface of the proximal sesamoid bones could be well identified. The cartilage at the most distal part of the sagittal ridge and the condyles of MCIII and the cartilage of the proximal phalanx were difficult to see or was even not visible on the transverse, sagittal, and dorsal planes. The proximal synovial pad of the articular capsule could be clearly assessed on the sagittal and transverse postcontrast image.

Discussion

The present investigation was carried out to characterize the anatomic features of the MCP joint in horses by use of multidetector row CT. Multidetector row CT, compared with convential axial CT, substantially improves visualization of small structures. Improvements are attributed to the thinner collimation, faster scanning, higher spatial resolution, decrease in noise, and larger number of images generated during the same scanning time.[19]

Results of the study indicated that not only the bony structures but also the clinically important soft tissue structures could be well identified by use of CT. Computed tomography has proven its usefulness in the diagnosis of subchondral bone cysts,[8] osteomyelitis of the axial border of the proximal sesamoid bones,[4–6,8] condylar fractures,[20] palmar subchondral bone lesions, and small osteochondral fragments.[21,h] Computed tomography is an excellent imaging modality for evaluation of bony structures. In the present study, CT provided excellent discrimination between the cortex and medulla of MCIII, the proximal sesamoid bones, and the proximal phalanx.

A difference in bone density distribution in relation to the imputed compressive load path is present between trained 2-year-old Thoroughbred racehorses and untrained horses. A zone of increased density (sclerosis) extends from the distopalmar aspect obliquely across the epiphysis to its dorsoproximal surface, leaving an area of lesser density at the most dorsodistal aspect of the condyle in trained horses.[22] The most radiodense bone is located in the subchondral and underlying regions of the palmar aspects of both condyles, whereas bone deep to the sagittal ridge on the palmar aspect is less dense in Thoroughbred racehorses.[23] In normal condyles, the palmar aspect of the lateral condyle is denser, compared with the medial condyle; in condyles affected by osteoarthritis, the dorsal aspect and medial condyle have the most dense bone.[16,23] This pattern, which occurs in trained Thoroughbred racehorses, was not observed in horses in this study probably because we used nonracehorses of a mean age of 13 years.

Detailed views of the soft tissue structures were attainable by use of the correct window setting (WW = 280 HU; WL = 120 HU). The dorsal and sagittal planes were reconstructed with a slice thickness of 2 mm for visualization of the soft tissues. The transverse planes were reformatted from the transverse acquisition (thickness, 1 mm) with a slice thickness of 2 mm. This was done to decrease the image noise present on the transverse images with a slice thickness of 1 mm.

The accessory digital extensor tendon arises lateral to the common digital extensor muscle at the level of the carpus and joins the lateral digital extensor tendon at the level of MCIII thus lying medial, near midline relative to the lateral digital extensor tendon.[24] However, it is not an uncommon finding that this small tendon remains separate and continues just to the proximal phalanx.[25] In 3 of the 4 forelimbs, the accessory digital extensor tendon was still present at the level of the MCP joint.

The straight distal sesamoidean ligament had a heterogeneous appearance in its middle portion, compared with its appearance at the origin and insertion. The oblique distal sesamoidean ligaments also had a heterogeneous appearance throughout their length. This is, in both ligaments, the result of loose connective tissue fibers (including adipose tissue) between the ligament fibers.[26] The heterogeneous appearance of the straight distal sesamoidean ligament was also probably attributable to relaxation of the ligament when the foot is not in a weight-bearing position, and this should not be misinterpreted as a lesion. If there is doubt regarding the presence of a lesion, intra-arterial contrast-enhanced CT can be performed.[17] Because of the heterogeneous appearance of the straight distal sesamoidean ligament, the sagittal part of the oblique distal sesamoidean ligament was almost not distinguishable from the straight distal sesamoidean ligament.

Differentiation between the superficial and deep parts of the collateral ligaments of the MCP joint could not be made. Because of their attachment sites, separation at those sites was a possibility. This is in agreement with results of CT of the carpus,[12] where the separation of the collateral ligaments could also not be detected, and with results of MRI of the collateral ligaments of the tarsus (other than known origin and insertion points).[27] In contrast, by use of CT, the distinction of the medial and lateral collateral ligaments into a short

and long division at the tarsus was made.[28] Differentiation between the cruciate, oblique, and straight distal sesamoidean ligaments and between the short and oblique sesamoidean ligaments at their origin site on the proximal sesamoid bones could not be made on the sagittal reconstructions as well as differentiation between the sagittal part of the oblique distal sesamoidean ligament and straight distal sesamoidean ligament on the transverse planes and between the collateral sesamoidean ligaments and superficial part of the collateral ligaments. Differentiation between the short and oblique distal sesamoidean ligaments on the transverse images was difficult. Separation of structures with the same density, such as the short, cruciate, oblique, and straight sesamoidean ligaments; the superficial and deep part of the collateral ligaments; and the collateral sesamoidean ligaments with the superficial part of the collateral ligaments, remains difficult with CT.[10]

In a previous study[29] of MRI of the MCP joint, the sagittal plane was chosen rather than the transverse or dorsal planes because it was believed to contain more tissue types than would the other 2 planes and because sagittal planes provided information about the tissues in an orientation more recognizable than transverse images. Previous studies[27,30] involving MRI of the tarsus and foot revealed that the sagittal and the transverse planes provided the most complete visualization of the most clinically important anatomic structures. This is in agreement with our study for most structures of the MCP joint. However, in our study, the dorsal reconstructions were useful for evaluation of the collateral ligaments and the attachment sites of the straight distal and oblique distal sesamoidean ligaments on the proximal sesamoid bones.

The cartilage of the MCP joint can be visualized by use of CT arthrography, although the sensitivity of the visualization of artificial cartilage lesions was as low as 31%, depending on the location (dorsal part of MCIII, palmar part of MCIII, or sesamoid bones) and the size (superficial cartilage lesions vs cartilage lesions with subchondral bone involvement) of the lesions in cadavers, and 58% in patients.[a] By use of MRI, the sagittal plane was the most useful for evaluation of the articular cartilage of the distal aspect of the metacarpus, the proximal portion of the proximal phalanx, and the dorsal margin of the proximal sesamoid bones.[29] In our CT investigation, the transverse and sagittal planes were useful for identification of cartilage. The cartilage at the most distal part of the sagittal ridge and the condyles and the cartilage of the proximal phalanx were difficult to see or not visible in the transverse, sagittal, and dorsal planes. This was probably attributable to the decrease in thickness of cartilage from proximal (approx 1 mm) to distal (approx 0.5 mm),[31] which leads to insufficient resolution at that level.

The choice of the best imaging plane is certainly determined by the clinical findings. Ideally, all 3 planes (transverse planes and sagittal and dorsal reconstructions) should be acquired or reformatted for a complete CT examination of the MCP joint.

Computed tomography allowed a full assessment of the MCP joint because of the good soft tissue and bone images that were obtained at the same time. Therefore, knowledge of the normal anatomy is essential, and results of the present study could be used as a basis for evaluation of CT images of the limbs of horses with MCP joint injuries.

a. Vymeister C. *Computertomographische Arthrographie des Knorpels und von Knorpel-läsionen in Fesselgelenk des Pferdes*. PhD dissertation, Tierärztliche Hochschule, Hannover, Germany, 2002.
b. T61, Hoechst Roussel Vet GmbH, Unterschleissheim, Germany.
c. Somatom Sensation 16, Siemens Medical Solutions, Forcheim, Germany.
d. Ioversol, G Optiray 350, Guerbet, BP 50400, F-95943 Roissy CdG Cedex, situé 16, rue J. Chaptal, F93600 Aulnay, France.
e. Syngo CT 2006G, ICS VB28B, Siemens, Munich, Germany.
f. Technovit T 7143, Kulzer, Wehrheim, Germany.
g. Electric band saw, Eureka, Saviolo Lelio Snc, Coriano, Italy.
h. Thomas HL, Galuppo LD, Wisner ER, et al. Computed tomography for identification of early third metacarpal traumatic palmar subchondral bone lesions (abstr), in *Proceedings*. Annu Sci Meet Am Coll Vet Radiol 2004;64.

References

1. Bienert A, Stadler P. Computed tomographic examination of the locomotor apparatus of horses—a review. *Pferdeheilk* 2006;22:218–226.
2. Denoix JM, Jacot S, Bousseau B, et al. Ultrasonographic anatomy of the dorsal and abaxial aspects of the equine fetlock. *Equine Vet J* 1996;28:54–62.
3. Ueltschi G, Voswinkel K, Lauk HD. Scintigraphical and radiological examination of fetlock joints in clinically sound and lame horses. *Pferdeheilk* 1996;12:25–32.
4. Barbee DD, Allen JR, Grant BD, et al. Detection by computed tomography of occult osteochondral defects in the fetlock of a horse. *Equine Vet J* 1987;19:556–558.
5. Wisner ER, O'Brien TR, Pool RR, et al. Osteomyelitis of the axial border of the proximal sesamoid bones in seven horses. *Equine Vet J* 1991;23:383–389.
6. Hanson JA, Seeherman HJ, Kirker-Head CA, et al. The role of computed tomography in evaluation of subchondral osseous lesions in seven horses with chronic synovitis. *Equine Vet J* 1996;28:480–488.
7. Kraft SL, Gavin P. Physical principles and technical considerations for equine computed tomography and magnetic resonance imaging. *Vet Clin North Am Equine Pract* 2001;17:115–130.
8. Rijkenhuizen ABM, van den Top GB, van den Belt AJ. The role of computed tomography in the surgical management of cystic lesions. *Pferdeheilk* 2005;21:317–321.
9. Tietje S. The value of computed tomography in horses (243 cases). 2. Diseases of the limbs. *Prakt Tierarzt* 1997;78:35–43.
10. Tucker RL, Sande RD. Computed tomography and magnetic resonance imaging of equine musculoskeletal conditions. *Vet Clin North Am Equine Pract* 2001;17:145–157.
11. Kaneps AJ, Koblick PD, Freeman DM, et al. Comparison of radiography, computed-tomography, and magnetic-resonance-imaging for the diagnosis of palmar process fractures in foals. *Vet Radiol Ultrasound* 1995;36:467–477.
12. Kaser-Hotz B, Sartoretti-Schefer S, Weiss R. Computed tomography and magnetic resonance imaging of the normal equine carpus. *Vet Radiol Ultrasound* 1994;35:457–461.
13. Mair TS, Kinns J, Jones RD, et al. Magnetic resonance imaging of the distal limb of the standing horse. *Equine Vet Educ* 2005;17:74–78.
14. Murray R, Mair T. Use of magnetic resonance imaging in lameness diagnosis in the horse. *In Pract* 2005;27:138–146.
15. Young BD, Samii VF, Mattoon JS, et al. Subchondral bone density and cartilage degeneration patterns in osteoarthritic metacarpal condyles of horses. *Am J Vet Res* 2007;68:841–849.
16. Collins JN, Galuppo LD, Thomas HL, et al. Use of computed tomography angiography to evaluate the vascular anatomy of the distal portion of the forelimb of horses. *Am J Vet Res* 2004;65:1409–1420.

17. Puchalski SM, Galuppo LD, Hornof WJ, et al. Intraarterial contrast-enhanced computed tomography of the equine distal extremity. *Vet Radiol Ultrasound* 2007;48:21–29.
18. Denoix JM. *The equine distal limb: an atlas of clinical anatomy and comparative imaging*. London: Manson Publishing, 2000.
19. Berland LL, Smith JK. Multidetector-array CT: once again, technology creates new opportunities. *Radiology* 1998;209:327–329.
20. Morgan JW, Santschi EM, Zekas LJ, et al. Comparison of radiography and computed tomography to evaluate metacarpo/metatarsophalangeal joint pathology of paired limbs of thoroughbred racehorses with severe condylar fracture. *Vet Surg* 2006;35:611–617.
21. Kawcak CE, McIlwraith CW, Norrdin RW, et al. Clinical effects of exercise on subchondral bone of carpal and metacarpophalangeal joints in horses. *Am J Vet Res* 2000;61:1252–1258.
22. Firth EC, Rogers CW, Doube M, et al. Musculoskeletal responses of 2-year-old Thoroughbred horses to early training. 6. Bone parameters in the third metacarpal and third metatarsal bones. *N Z Vet J* 2005;53:101–112.
23. Riggs CM, Whitehouse GH, Boyde A. Structural variation of the distal condyles of the third metacarpal and third metatarsal bones in the horse. *Equine Vet J* 1999;31:130–139.
24. Seiferle E, Frewein J. Active locomotor system, muscular system, myologia. In: Nickel R, Schummer A, Seiferle E, et al, eds. *The anatomy of the domestic animals. Volume 1. The locomotor system of the domestic mammals*. Berlin-Hamburg: Verlag Paul Parey,1986;214–466.
25. Barone R. Muscles de la ceinture et du membre thoraciques. In: Barone R, ed. *Anatomie comparée des mammifères domestiques. Tome 2. Arthrologie et myologie*. 4th ed. Paris: Editions Vigot, 2000;719–842.
26. Kleiter M, Kneissl S, Stanek C, et al. Evaluation of magnetic resonance imaging techniques in the equine digit. *Vet Radiol Ultrasound* 1999;40:15–22.
27. Blaik MA, Hanson RR, Kincaid SA, et al. Low-field magnetic resonance imaging of the equine tarsus: normal anatomy. *Vet Radiol Ultrasound* 2000;41:131–141.
28. Tomlinson JE, Redding WR, Berry C, et al. Computed tomographic anatomy of the equine tarsus. *Vet Radiol Ultrasound* 2003;44:174–178.
29. Martinelli MJ, Baker GJ, Clarkson RB, et al. Correlation between anatomic features and low-field magnetic resonance imaging of the equine metacarpophalangeal joint. *Am J Vet Res* 1996;57:1421–1426.
30. Dyson S, Murray R, Schramme M, et al. Magnetic resonance imaging of the equine foot: 15 horses. *Equine Vet J* 2003;35:18–26.
31. Denoix JM, Audigie F. Ultrasonographic examination of joint in horses, in *Proceedings*. 47th Proc Am Assoc Equine Pract 2001;366–375.
32. Dyson SJ, Denoix JM. Tendon, tendon sheath, and ligament injuries in the pastern. *Vet Clin North Am Equine Pract* 1995;11:217–233.